THE JOURNAL OF BIOLOGICAL CHEMISTRY
Vol. 278, No. 48, Issue of November 28, pp. 48146–48153, 2003
Printed in U.S.A.

Structural Properties of Gerstmann-Sträussler-Scheinker Disease Amyloid Protein*

Received for publication, July 8, 2003, and in revised form, September 5, 2003
Published, JBC Papers in Press, September 11, 2003, DOI 10.1074/jbc.M307295200

Mario Salmona‡§, Michela Morbin¶, Tania Massignan‡, Laura Colombo‡, Giulia Mazzoleni¶, Raffaella Capobianco¶, Luisa Diomede‡, Florian Thaler‡, Luca Mollica‡, Giovanna Musco‖, Joseph J. Kourie, Orso Bugiani¶, Deepak Sharma‡‡, Hideyo Inouye‡‡, Daniel A. Kirschner‡‡§§, Gianluigi Forloni‡, and Fabrizio Tagliavini¶**

*From the ‡Istituto di Ricerche Farmacologiche "Mario Negri," Via Eritrea 62, 20157 Milan, ¶Istituto Nazionale Neurologico "Carlo Besta," Via Celoria 11, 20133 Milan, ‖Dulbecco Telethon Institute, Neurobiologia Cellulare e Molecolare c/o DIBIT, Via Olgettina 58, 20132 Milan, Italy, **Membrane Transport Group, Department of Chemistry, Science Road, The Australian National University, Canberra City, ACT 0200, Australia, and ‡‡Biology Department, Boston College, Chestnut Hill, Massachusetts 02467-3811*

Prion protein (PrP) amyloid formation is a central feature of genetic and acquired forms of prion disease such as Gerstmann-Sträussler-Scheinker disease (GSS) and variant Creutzfeldt-Jakob disease. The major component of GSS amyloid is a PrP fragment spanning residues ~82–146. To investigate the determinants of the physicochemical properties of this fragment, we synthesized PrP-(82–146) and variants thereof, including entirely and partially scrambled peptides. PrP-(82–146) readily formed aggregates that were partially resistant to protease digestion. Peptide assemblies consisted of 9.8-nm-diameter fibrils having a parallel cross-β-structure. Second derivative of infrared spectra indicated that PrP-(82–146) aggregates are primarily composed of β-sheet (54%) and turn (24%) which is consistent with their amyloid-like properties. The peptide induced a remarkable increase in plasma membrane microviscosity of primary neurons. Modification of the amino acid sequence 106–126 caused a striking increase in aggregation rate, with formation of large amount of protease-resistant amorphous material and relatively few amyloid fibrils. Alteration of the 127–146 region had even more profound effects, with the inability to generate amyloid fibrils. These data indicate that the intrinsic properties of PrP-(82–146) are dependent upon the integrity of the C-terminal region and account for the massive deposition of PrP amyloid in GSS.

The molecular signature of prion diseases is a post-translational modification of the prion protein (PrP)[1] from a normal cellular isoform (PrP^C) to disease-specific species (PrP^{Sc}) (1, 2). The transition from PrP^C to PrP^{Sc} involves conformational changes with decrease in α-helical secondary structure and significant increase in β-sheet content (3–5). This rearrangement is accompanied by the acquisition of abnormal physicochemical properties including insolubility in non-denaturing detergents and partial resistance to proteinase K (PK) digestion (1). In the presence of detergents, the protease-resistant core of PrP^{Sc} assembles into insoluble fibrillar structures with the tinctorial and ultrastructural properties of amyloid (6). PrP amyloidogenesis occurs consistently in genetic forms of disease, such as Gerstmann-Sträussler-Scheinker (GSS) disease and PrP cerebral amyloid angiopathy (7, 8), and in the new variant of Creutzfeldt-Jakob disease that is causally linked to bovine spongiform encephalopathy (9, 10). In all these conditions, amyloid fibrils are associated with PrP aggregates that are devoid of the tinctorial and ultrastructural properties of amyloid (11), suggesting that different PrP peptides or protein conformers may trigger fibrillar or non-fibrillar aggregates. Biochemical studies have shown that amyloid fibrils purified from GSS brain contain a major PrP fragment of ~7 kDa, spanning residues 81–82 to 144–153 of PrP (12, 14). This fragment is very similar in patients with different mutations (*i.e.* A117V, F198S, Q217R) and is derived from mutant PrP, although in GSS F198S and Q217R it does not contain the amino acid substitution (13). Evidence suggests that N- and C-terminal cleavage of abnormal PrP isoforms generating amyloid peptides occurs before rather than after fibril formation (15). Western blot analysis of total brain extracts from F198S patients has revealed three major protease-resistant PrP fragments of 27–29, 18–19, and 8 kDa. The 18–19- and 8-kDa peptides are N- and C-terminal truncated, as deduced by their antigenic profile, and are unglycosylated, likely representing amyloid protein precursors (15). Similar low molecular weight fragments have been detected in GSS patients with other *PRNP* mutations and are also present in areas without amyloid deposits, suggesting that regional factors feature in amyloidogenesis (15–17). Of note, the PrP region spanning residues 89–140 is an integral part of the minimal sequence which sustains prion replication (18, 19), suggesting that it plays a central role in the conformational transition of PrP^C into PrP^{Sc} and in PrP^{Sc} propagation.

To investigate the contribution of different regions of the GSS amyloid protein to the physicochemical properties of disease-specific PrP isoforms and fibrillogenesis, we synthesized a peptide homologous to the smallest amyloid subunit purified from GSS brains ($PrP\text{-}(82–146)_{wt}$) and PrP peptides with scrambled sequences thereof. In particular, we generated an

* This work was supported in part by Italian Ministry of Health Grant RF 2001.96, Italian Ministry of University and Research Grant PRIN 2001, European Union Grant QLRT 2001-00283, an Alzheimer's Association/T.L.L. Temple Discovery Award (to D. A. K.), and by institutional support from Boston College. The costs of publication of this article were defrayed in part by the payment of page charges. This article must therefore be hereby marked "*advertisement*" in accordance with 18 U.S.C. Section 1734 solely to indicate this fact.

§ To whom correspondence should be addressed. Tel.: 39-02-39210812; Fax: 39-02-3546277; E-mail: salmona@marionegri.it.

§§ Recipient of a Fulbright Senior Research Scholar award from the Binational United States-Italian Fulbright Scholar Program.

[1] The abbreviations used are: PrP, prion protein; FTIR, Fourier transform IR; GSS, Gerstmann-Sträussler-Scheinker; PK, proteinase K; HPLC, high pressure liquid chromatography; EM, electron microscopy; FP, fluorescence polarization; DPH, 1,6-diphenyl-1,3,5-hexatriene.

entirely scrambled PrP-(82–146) (PrP-$(82–146)_{scr}$) and partially scrambled PrP-(82–146), where only the sequence 106–126 (PrP-$(82–146)_{106–126scr}$) or 127–146 (PrP-$(82–146)_{127–146scr}$) was altered (Fig. 1). The selection of the sequences to be modified was based on previous observations that the region spanning residues 106–147 is central to amyloid fibril formation (20). In particular, a peptide comprising residues 106–126 showed high propensity to adopt stable β-sheet secondary structure and to assemble into straight, unbranched amyloid fibrils, similar in ultrastructure to those observed in GSS patients (20–22). Also, a peptide spanning PrP residues 127–147 (PrP-(127–147)) was able to generate amyloid-like fibrils, resembling scrapie-associated fibrils isolated from subjects with transmissible spongiform encephalopathies (20). Here we report that PrP-$(82–146)_{wt}$ has high intrinsic ability to form amyloid fibrils indistinguishable from those observed in GSS disease and that the formation of ordered structures having a parallel β-sheet organization is dependent upon the integrity of the C-terminal region.

MATERIALS AND METHODS

Synthesis and Purification of PrP Peptides—The following peptides were chemically synthesized: PrP-(82–146) wild type (PrP-$(82–146)_{wt}$, GQPHGGGWGQGGGTHSQWNKPSKPKTNMKHMAGAAAAGAVVG-GLGGYMLGSAMSRPIIHFGSDYE); PrP-(82–146) with a scrambled sequence in the region spanning residues 106–126 (PrP-$(82–146)_{106–126scr}$, GQPHGGGWGQGGGTHSQWNKPSKPNGAKALM-GGHGATKVVGAAAGYMLGSAMSRPIIHFGSDYE); PrP-(82–146) with a scrambled sequence in the region spanning residues 127–146 (PrP-$(82–146)_{127–146scr}$, GQPHGGGWGQGGGTHSQWNKPSKPKTN-MKHMAGAAAAGAVVGGLGSMYPASHGLMEDFYGIGSIR); PrP-(82–146) with a totally scrambled sequence (PrP-$(82–146)_{scr}$, EADQF-ALGGSKHGNGMQQVAGHGGSMGAKAWGANGHPSGTGIPTAKM-VPYKIYGGGWAGMGRPSS). In some experiments, the shorter peptides PrP-$(106–126)_{wt}$ (KTNMKHMAGAAAAGAVVGGLG) and PrP-$(127–146)_{wt}$ (GYMLGSAMSRTIIHFGSDYE) were also used. Peptides were prepared by solid-phase synthesis on a 433A synthesizer (Applied Biosystems, Foster City, CA) purified by reverse phase-HPLC and verified by amino acid sequencing (46600 Prosequencer, Milligen, Bedford, MA) and electrospray mass spectrometry (model 5989A, Hewlett-Packard, Palo Alto, CA) as described previously (22, 23).

Hydropathic Profile and Transmembrane Helix Prediction of PrP Peptides—PrP-$(82–146)_{wt}$ and its analogues were analyzed by a program devised by Kyte and Doolittle (24) that progressively evaluates the hydrophilicity and hydrophobicity of a protein along its amino acid sequence (www.expasy.ch/cgi-bin/protscale.pl). The common hydropathy value, defined at one specific position in a sequence, is the mean value of the hydrophobicity of the amino acids within a window around each position. In hydrophobic regions the hydropathy value is high for a number of consecutive positions in the sequence. The grand average of hydropathicity (GRAVY) is defined as the average value of the hydropathy value at each position (24). For prediction of membrane protein topology the TMHMM method, based on a hidden Markov model developed by Krogh and co-workers, was applied (25) (www.cbs.dtu.dk/services/TMHMM/).

Preparation of PrP Peptide Stock Solutions—Peptides were dissolved in sterile deionized water at 5 mg/ml. Under these conditions they were soluble, as deduced by the absence of a visible pellet after centrifugation at 13,000 × *g* for 10 min. The stock solutions were stable for 2 weeks at −80 °C, as determined by reverse phase-HPLC. For all the experiments aliquots of stock solutions were diluted with different buffers as specified below.

Sedimentation Experiments—The study was performed with 0.5 and 1 mM peptide in 20 mM Tris-HCl, pH 7.0. Aliquots of 30 μl were incubated at 37 °C for 1, 4, 8, 24, 48, 72, and 168 h and then chilled on ice and centrifuged at 13,000 × *g* for 10 min at 4 °C. Supernatants were analyzed by reverse phase-HPLC, and peptide concentrations at different times were expressed as percentages of the corresponding values determined at zero time (26).

PK Digestion—Aliquots of 1 mM peptides in 100 mM Tris-HCl, pH 7.0, containing 1 mM $CaCl_2$ were incubated at 37 °C for 96 h and then digested with PK for 30 min at 1:20 (w/w) enzyme-to-substrate ratio. Proteolysis was terminated by the addition of EGTA at a final concentration of 5 mM. After centrifugation at 13,000 × *g* for 10 min at 4 °C, the pellets were dissolved in 30 μl of 97% formic acid, and 20 μl were analyzed by reverse phase-HPLC. Control samples were processed under the same conditions in the absence of PK. The extent of the proteolysis was calculated as the percentage of the peptide present in the pellets compared with undigested controls (23).

Light and Electron Microscopy—Samples of 0.5, 0.1, and 0.05 mM peptides in 50 mM Tris-HCl, pH 7.0, were incubated at 37 °C for 1, 4, 8, 24, 48, 72, and 168 h. At each time point, sample aliquots were analyzed by light and electron microscopy. For light microscopy, 10 μl of suspension were air-dried on poly-L-lysine-coated slides (Bio-Optica, Milan, Italy), stained with thioflavine S and Congo Red, and viewed under fluorescent or polarized light, respectively (Nikon Eclipse E-800, Kyoto, Japan). For ultrastructural examination, 5 μl of suspension were applied to Formvar-carbon 200-mesh nickel grids for 5 min, negatively stained with uranyl acetate, and observed in an electron microscope (EM109 Zeiss, Oberkoken, Germany) operated at 80 kV at a standard magnification, calibrated with an appropriate grid. The mean diameter of fibrils generated by PrP peptides after short (1 h) and long (1, 3, and 7 days) incubation was measured on printed photos at a final magnification of ×90,000 by using a computer-assisted image analyzer (Nikon, Japan) (23).

At day 7, samples were centrifuged at 13,000 × *g* for 15 min. The pellets were fixed in 2.5% glutaraldehyde in 50 mM phosphate buffer, pH 7.4, post-fixed in 0.1% aqueous osmium tetroxide, dehydrated in graded acetone, and embedded in epoxy resin (Spurr, Electron Microscopy Science, Fort Washington, PA). Ultrathin sections (50 nm) were collected on 200-mesh copper grids, positively stained with uranyl acetate and lead citrate, and observed with the electron microscope.

X-ray Diffraction—The peptides were analyzed under the following conditions: lyophilized, vapor-hydrated, solubilized, and then dried. Lyophilized peptide was gently packed into a siliconized thin walled glass capillary (0.7 mm diameter; Charles A. Supper Co., South Natick, MA) to form a disk. For vapor hydration, the lyophilized peptide was equilibrated against a column of water that was sealed with it in the capillary. For preparing solubilized/dried peptide assemblies, lyophilized peptide was dissolved at ~10 mg/ml in water, and the solution was aspirated into a thin walled siliconized capillary to a column height of ~10–12 mm. A tiny hole was poked through the sealing wax at one end of the capillary, and the sample was left to dry gradually under ambient temperature and humidity while in a 2-tesla permanent magnet (Charles A. Supper Co.) (27), which can promote fibril alignment by diamagnetic anisotropy (28). Orientation and dehydration were monitored by periodic observation of sample birefringence between crossed polarizers. When the sample had dried to a small uniform disk, the capillary was transferred to a holder for x-ray diffraction.

X-ray diffraction patterns were obtained using nickel-filtered, double-mirror focused CuK_{α} radiation from an Elliott GX-20 rotating anode x-ray generator (GEC Avionics, Hertfordshire, UK) with a 200-μm focal spot, operated at 35 kV and 25 mA. A helium tunnel was placed in the x-ray path to reduce air scatter. Patterns were recorded on Eastman Kodak DEF film. The known Bragg spacing of calcite (0.3035 nm) was used to calibrate the specimen-to-film distance (87.6 mm). The Bragg spacings of reflections were measured with a 6× optical comparator directly off the films.

FTIR of Peptide Aggregates—Samples of 0.1 mM PrP-$(82–146)_{wt}$ and PrP-$(82–146)_{106–126scr}$ in 20 mM Tris-HCl, pH 7.0, were incubated at 37 °C for 24 h. Following centrifugation at 3,000 × *g* for 10 min, peptide aggregates were collected and gently dried in a stream of nitrogen to remove any water residue. The samples were mixed with KBr, pulverized, and formed into a disk-shaped pellet (29, 30). Data were collected on the solid pellets at room temperature with a Fourier transform IR spectrum BX (PerkinElmer Life Sciences) for wavelengths in the range of 4000 to 400 cm^{-1}. The spectral processing and the determination of the secondary structures from the intensities of bands in the second derivative amide I spectra were performed as described by Caughey *et al.* (3). As indicated by the relatively small signal of the second derivative spectrum in the range 1720–1800 cm^{-1} (Fig. 8*A*, *inset*), there was little or no appreciable residual water vapor contribution to the spectrum, and the signal-to-noise was sufficiently high for the secondary structure determination.

Membrane Microviscosity Determination—Membrane microviscosity was assessed in suspensions of primary cultures of rat cortical neurons using DPH as a fluorescent probe as described previously (31). The reported FP (expressed as arbitrary units) is a function of the emission (420 nm) detected through an analyzer oriented parallel (p_1) and perpendicular (p_2) to the direction of the polarization of the exciting light (365 nm), according to the equation $FP = (p_2 - p_1)/(p_2 + p_1)$ (12). Membrane microviscosity (η, poise) is related to FP according to the equation $\eta = 2FP/0.46 - FP$. Neuronal cells (2×10^6 cell/ml) were mechanically detached, gently centrifuged at 550 × *g* for 10 min, washed with saline, resuspended in 2.5 ml of 5 mM phosphate buffer, pH

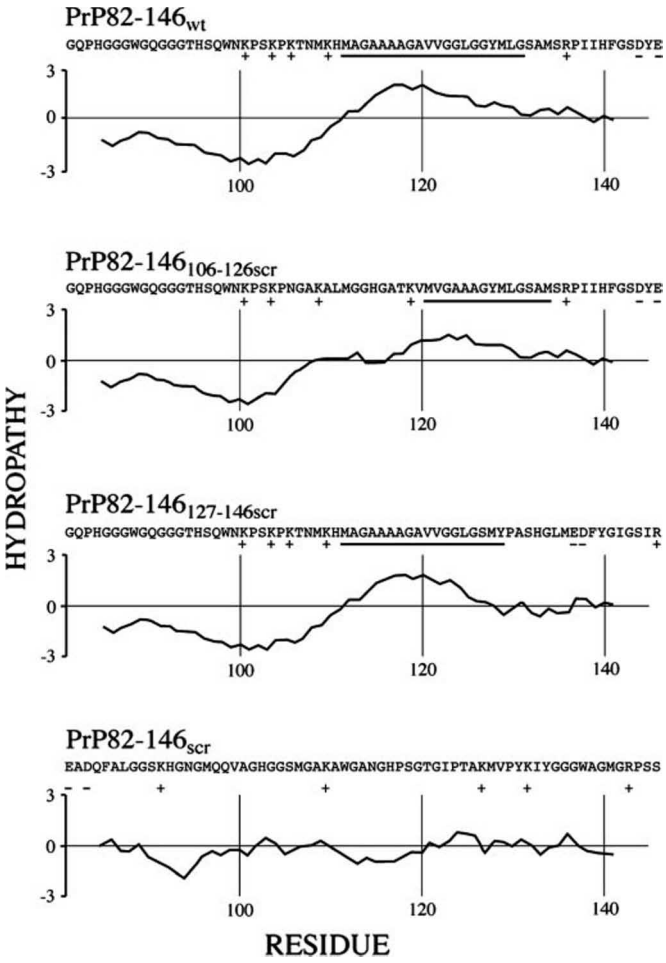

FIG. 1. **Primary structure, hydropathy plot and position of net charges of PrP-(82–146) and its analogues.** The potential transmembrane domains, as deduced by a membrane protein topology prediction method (36), are *underlined*.

7.4, containing 2 μM DPH, and incubated for 30 min at room temperature. PrP peptides were dissolved in 5 mM phosphate buffer, pH 7.4, and tested within 10 min of solubilization. The FP value was determined at 25 °C, before and 30 min after the addition of 25 μM PrP peptides to cell suspensions (31).

RESULTS

Hydropathic Profile of PrP-(82–146) Peptides—The hydropathic profile of the peptides selected for study was evaluated according to the Kyte and Doolittle scale (24). The analysis showed that PrP-$(82–146)_{wt}$ has an N-terminal hydrophilic region followed by an extended hydrophobic domain spanning residues 112–131, with a maximum of 1.844 at Gly-119 and a minimum of 0.633 at Gly-131. PrP-$(82–146)_{127–146scr}$ exhibited a similar profile, whereas the alteration of the 106–126 sequence (PrP-$(82–146)_{106–126scr}$) resulted in a shorter hydrophobic region spanning residues 120–131, with a maximum of 1.511 at Ala-124 and a minimum of 0.633 at Gly-131. PrP-$(82–146)_{scr}$ showed a flat profile, consistent with its disarranged hydrophilic and hydrophobic domains compared with PrP-$(82–146)_{wt}$ (Fig. 1).

Disarrangement of C-terminal Region of PrP-(82–146) Has Profound Effect on Peptide Aggregation—To investigate the ability of PrP-$(82–146)_{wt}$ and its analogues to form macroaggregates, we carried out sedimentation experiments. Peptides were dissolved in 20 mM Tris-HCl, pH 7.0, incubated at 37 °C for 0–96 h, and then centrifuged. The supernatants were analyzed by HPLC to determine the percentage of peptide still in solution after centrifugation. The aggregation kinetics of PrP-$(82–146)_{wt}$ was substantially linear during the first 3 days, yielding ~25, 40, and 60% of sedimentable peptide after 24, 48, and 72 h, respectively. Thereafter, the peptide showed an increased aggregation rate, and more than 90% was found in the pellet after 96 h. The modification of the amino acid sequence 106–126 resulted in a change in the aggregation kinetics, as almost 60% of PrP-$(82–146)_{106–126scr}$ was sedimentable after 24 h; subsequently, the aggregation proceeded slowly, except for an acceleration in the last 24 h leading to more than 85% of sedimentable peptide after 96 h of incubation. On the other hand, the alteration of the 127–146 region remarkably reduced the aggregation ability, as PrP-$(82–146)_{127–146scr}$ showed a limited rate of assembly into sedimentable structures that reached statistical significance ($t < 0.01$, Student's t test, $n = 5$) in comparison to the non-sedimentable PrP-$(82–146)_{scr}$ only after 96 h (Fig. 2).

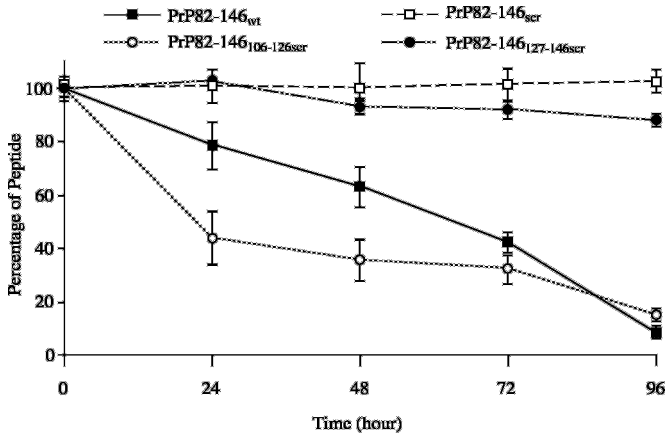

FIG. 2. **Time course of PrP peptides aggregation.** Peptides were dissolved in 20 mM Tris-HCl, pH 7.0, at the concentration of 0.5 mM and incubated for 0–96 h at 37 °C. Following centrifugation, the supernatants were analyzed by HPLC. The non-sedimentable peptide fraction was expressed as percentage of the total amount of peptide at time 0. Each value is the mean ± S.D. of at least five experiments.

Protease Resistance of PrP Peptides Related to Their Aggregation Properties—Suspensions of pre-aggregated peptides were subjected to PK digestion at 37 °C for 30 min at 1:20 (w/w) enzyme-to-substrate ratio. Following centrifugation, the pellets were dissolved in formic acid and analyzed by HPLC. The extent of proteolysis was calculated as percentage of peptide present in the pellet compared with undigested controls. Under these conditions, 47.2 ± 3.0% of PrP-$(82–146)_{wt}$ was protease-resistant, whereas PrP-$(82–146)_{scr}$ was almost completely degraded (Fig. 3). The modification of the amino acid sequence 127–146 resulted in a decrease of the protease-resistant fraction to 15.4 ± 2.3% of control values. Conversely, the change of the 106–126 region yielded a striking increase in PK resistance (78.3 ± 8.2%).

PrP-(82–146) Protofilament and Amyloid Fibril Formation Depends upon Integrity of C-terminal Region—The staining properties and ultrastructure of aggregates generated by PrP-(82–146) analogues were determined at various incubation times ranging from 1 to 168 h. At each time point, aliquots of peptide suspensions were stained with Congo Red and thioflavine S and examined by polarized light and fluorescence microscopy, respectively, or negatively stained with uranyl acetate and analyzed by EM. After 168 h, the samples were centrifuged, and the pellets were fixed in glutaraldehyde and embedded in Spurr. Ultrathin sections were positively stained and analyzed by EM.

The analysis showed that PrP-$(82–146)_{wt}$ readily formed amyloid fibrils, whereas the entirely scrambled peptide, PrP-$(82–146)_{scr}$, did not generate filamentous structures even after

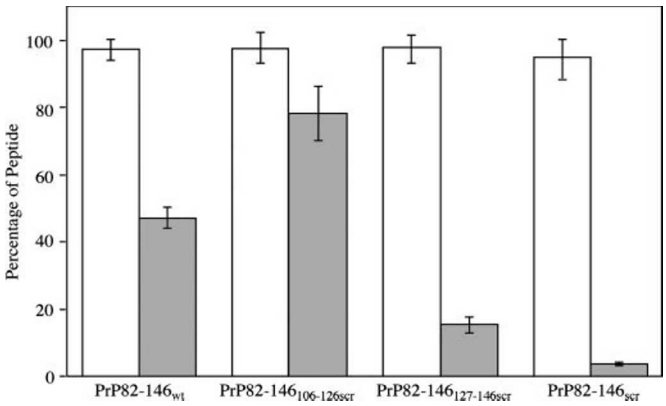

FIG. 3. **Protease resistance of PrP peptides.** Peptides were dissolved in 100 mM Tris-HCl, pH 7.0, containing 1 mM $CaCl_2$ at the concentration of 1 mM, and incubated at 37 °C for 96 h. They were then subjected to digestion with proteinase K for 30 min at 1:20 (w/w) enzyme-to-substrate ratio. Following centrifugation, pellets were dissolved in 97% formic acid and analyzed by HPLC. The extent of proteolysis was calculated as percentage of peptide present in the pellet. Each value is the mean ± S.D. of at least five experiments.

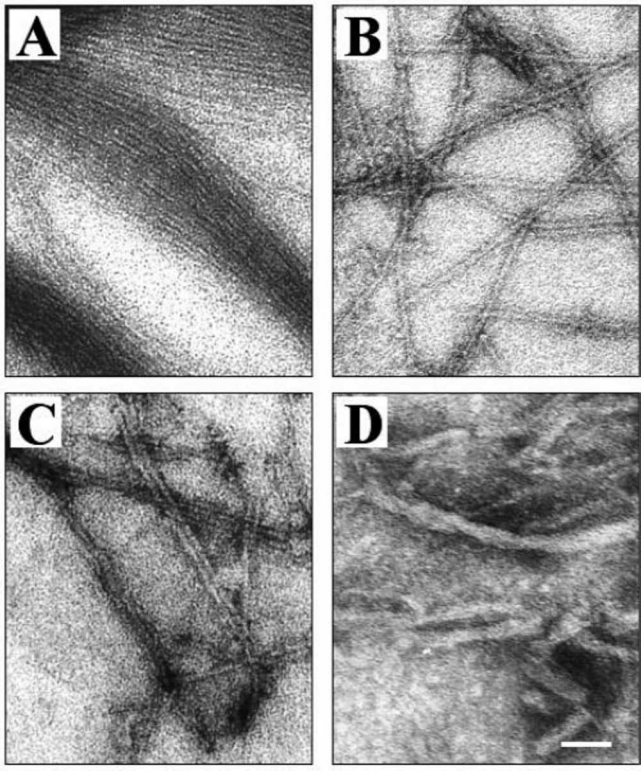

FIG. 4. **Electron micrographs of the aggregates generated by PrP-(82–146) analogues, as revealed by negative staining of peptide suspensions.** *A* and *B* show two distinct populations of fibrils generated by PrP-$(82–146)_{wt}$ after a 1-h incubation, whereas *C* and *D* correspond to PrP-$(82–146)_{106–126scr}$ and PrP-$(82–146)_{127–146scr}$ after a 48-h incubation, respectively. *Bar*, 100 nm.

a 7-day incubation. Two distinct populations of long, straight, unbranched fibrils were observed in negatively stained PrP-$(82–146)_{wt}$ suspensions after 1 h: (i) 5.5-nm-diameter protofilaments with high propensity to adhere to each other, organizing into bundles of various widths (Fig. 4*A*); and (ii) 9.5-nm-diameter fibrils generating loose meshworks (Fig. 4*B* and Table I). The first population progressively decreased, whereas the second population progressively increased with time, and only 9.8-nm-diameter fibrils organized into dense meshworks were detectable after 72 h.

TABLE I
Diameter (nm) of fibrils generated by PrP-(82-146) analogues at different incubation times

Results are the means ± S.D. of at least 100 measurements in three different experiments.

Time	PrP-$(82-146)_{wt}$	PrP-$(82-146)_{106-126scr}$	PrP-$(82-146)_{127-146scr}$
h			
1	5.5 ± 1.8 9.5 ± 1.1	No fibrils	No fibrils
24	5.6 ± 1.8 9.6 ± 1.2	7.3 ± 1.0	7.1 ± 1.5
72	9.7 ± 1.1	7.6 ± 0.9	7.3 ± 1.1
168	9.8 ± 1.1	7.7 ± 1.1	7.4 ± 1.0

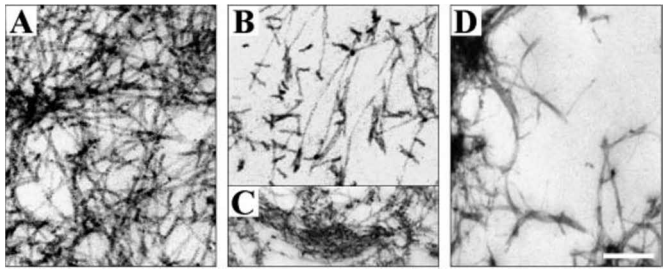

FIG. 5. **Electron micrographs of the aggregates generated by PrP-(82–146) analogues, as revealed by positive staining of ultrathin sections of the pellets obtained by centrifugation after 1 week of incubation.** *A*, PrP-$(82–146)_{wt}$; *B* and *C*, PrP-$(82–146)_{106–126scr}$; *D*, PrP-$(82–146)_{127–146scr}$. *Bar*, 100 nm.

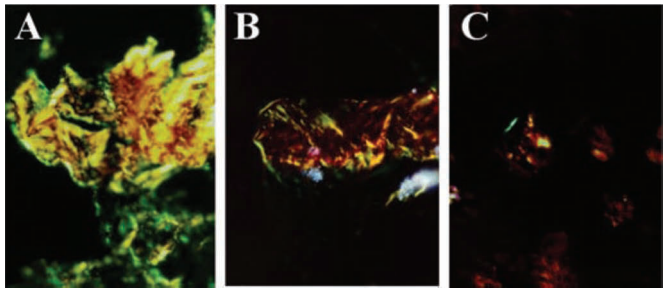

FIG. 6. **Congo Red staining of PrP peptide aggregates.** Peptide suspensions were incubated for 48 h and then analyzed by polarized light microscopy. *A*, PrP-$(82–146)_{wt}$; *B*, PrP-$(82–146)_{106–126scr}$; *C*, PrP-$(82–146)_{127–146scr}$.

The fibrillogenic ability of the peptide was affected by modification of the 106–126 region. After 1 h of incubation, PrP-$(82–146)_{106–126scr}$ generated primarily amorphous aggregates that were associated with few, relatively short, unbranched, irregular filaments having an average diameter of 7.3 nm. With time, the density of fibrillar assemblies progressively increased and more regular, straight, unbranched fibrils having a diameter of 7.7 nm were detected (Fig. 4*C* and Table I). These fibrils were often paired or organized into bundles or loose meshworks and were associated with a substantial amount of amorphous aggregates. Alteration of the 127–146 region had an even more profound effect. After 1 h of incubation, negatively stained samples of PrP-$(82–146)_{127–146scr}$ essentially contained some amorphous material. After 24 h, a few irregular threads and filamentous structures having a diameter of 7.1 nm were also present. The filaments increased with time and tended to adhere to each other, with formation of twisted bundles of various widths, depending on the number of the constituent filaments (Fig. 4*D* and Table I). However, even after 7 days, the samples largely consisted of amorphous material, and the overall density of the aggregates was remarkably lower than observed with PrP-$(82–146)_{wt}$ and PrP-$(82–146)_{106–126scr}$.

EM examination of the pellets obtained by centrifugation of

TABLE II
Summary of x-ray diffraction measurements

Sample[a]	82-146$_{wt}$			82-146$_{106-126scr}$			82-146$_{127-146scr}$	82-146$_{scr}$
Condition	L	VH	S/D	L	VH	S/D	S/D	S/D
Spacing[b]	0.484 C	0.477 C	0.477 M	0.469 C	–	0.473 C	–	0.278[c]
Forward scatter[d]	+	+	+5.9	+	–	+	–	–
Exposure (h)	43	40	70	72	22	141	106	118

[a] *L*, lyophilized; *VH*, vapor-hydrated; *S/D*, solubilized and dried.
[b] Bragg spacing in nm; *C*; circular reflection, *M*; meridional reflection. – indicates that discrete reflections were not detected.
[c] This crystalline, sharp reflection likely arises from NaCl.
[d] Forward scatter refers to the central scattering observed near the beam stop, likely arising from the structure factor of the macromolecular assembly. The solubilized and dried sample of PrP-(82-146)$_{wt}$ is the only sample that gave an oriented pattern. A broad and weak intensity maximum was observed at 5.9 nm Bragg spacing.

peptide suspensions after a 7-day incubation enabled a better definition of the fine morphology of different types of aggregates and the evaluation of their relative amount. Positively stained ultrathin sections of PrP-(82–146)$_{wt}$ contained only long, straight, unbranched fibrils that formed dense meshworks (Fig. 5*A*) or, less often, star-like structures whose morphology was very similar to human GSS amyloid plaques cores. Also, PrP-(82–146)$_{106-126scr}$ preparations contained straight, unbranched amyloid-like fibrils that could be distinguished from those of PrP-(82–146)$_{wt}$ by being smaller in diameter and shorter. Furthermore, the fibrillar assemblies were less dense (Fig. 5*B*) and were associated with a large amount of granular and amorphous material (Fig. 5*C*). The pellet obtained from PrP-(82–146)$_{127-146scr}$ was smaller than that generated by PrP-(82–146)$_{wt}$ and PrP-(82–146)$_{106-126scr}$ and contained primarily electron dense amorphous material intermingled with a relatively small number of short filamentous structures. PrP-(82–146)$_{127-146scr}$ filaments did not possess the ultrastructural features of amyloid fibrils and were usually assembled into twisted bundles (Fig. 5*D*).

Macromolecular assemblies of PrP-(82–146)$_{wt}$ showed the tinctorial and optical properties of *in situ* amyloid, *i.e.* birefringence under polarized light after Congo Red staining and yellow fluorescence after thioflavine S treatment. These properties were detected even after 1 h and were more apparent after longer incubation times, as the number and size of the aggregates increased (Fig. 6*A*). In PrP-(82–146)$_{106-126scr}$ samples, birefringent and fluorescent aggregates were observed only after 24 h and increased with time, without reaching the size and density of the wild type peptide even after 7 days (Fig. 6*B*). PrP-(82–146)$_{127-146scr}$ aggregates did not possess the tinctorial properties of amyloid, except for a few small bundles observed after long incubation (Fig. 6*C*).

PrP-(82–146)$_{wt}$ Fibrils Have Cross-β-structure—X-ray diffraction patterns were recorded from PrP-(82–146)$_{wt}$, PrP-(82–146)$_{106-126scr}$, PrP-(82–146)$_{127-146scr}$, and PrP-(82–146)$_{scr}$ peptides under three different conditions, *i.e.* lyophilized (L), vapor-hydrated (VH), and solubilized/dried (S/D) (Table II). PrP-(82–146)$_{wt}$ after the S/D treatment gave an oriented diffraction pattern where a sharp and strong reflection at Bragg spacing 0.477 nm was observed on the meridian (Fig. 7) and after L and VH treatments showed a circular reflection at ~0.47 nm. A similar circular reflection at ~0.47 nm was observed for PrP-(82–146)$_{106-126scr}$ after L and S/D treatments; conversely, the vapor-hydrated peptide did not show a distinct reflection, possibly due to the short exposure time. Neither PrP-(82–146)$_{127-146scr}$ nor PrP-(82–146)$_{scr}$ gave any distinct reflections, even after >100 h of exposure. The spacing at ~0.47 nm corresponds to the hydrogen-bonding distance between parallel or antiparallel β chains. The sharpness of this reflection indicates that the peptides form a periodic array of β chains that run normal to the long axis of the elongated assembly. An oriented sample of PrP-(82–146)$_{wt}$ after solubilization and drying showed a low angle reflection at 5.9 nm spacing. If this arises from the first intensity maximum of a long cylindrical (fibrillar) structure having radius r_0, the reciprocal coordinate R and r_0 are related by $2\pi r_0 R = 5.152$ for a solid cylinder and 3.770 for a tubular cylinder (32). Given $R = (5.9\ \text{nm})^{-1}$, the radius r_0 was calculated to be 4.8 nm for a solid cylinder and 3.5 nm for a tubular cylinder. Thus, the fibril diameter is ~7–10 nm. This estimate based on diffraction measurements was similar to the 9.7-nm width measured from electron micrographs of the second population of fibrils for PrP-(82–146)$_{wt}$. This size is larger than that of the protofilaments (4.0 nm) of a similar peptide (*i.e.* PrP-(90–145)) (33), indicating that the PrP-(82–146) fibril in the current study is likely constituted of a multiple of protofilaments. Unlike PrP-(82–146)$_{wt}$ orientation after S/D treatment, PrP-(82–146)$_{106-126scr}$ showed a weak circular reflection at ~0.47 nm, indicating lack of orientation and weaker scattering compared with the wild type peptide. Moreover, the larger breadth of the 0.47 nm reflection compared with that in the wild type suggests that the number of H-bonded strands is less in the structure formed by the scrambled sequence. PrP-(82–146)$_{127-146scr}$ and PrP-(82–146)$_{scr}$ did not show any distinct reflections, indicating that these peptides did not form a sufficient number of organized macromolecular assemblies that could be detected by x-ray scatter.

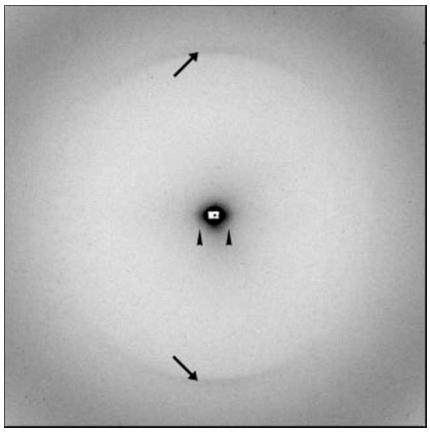

FIG. 7. **X-ray diffraction from PrP-(82–146)$_{wt}$ dried after solubilization and drying.** The exposure time was 70 h. The sharp meridional reflection had a Bragg spacing of 0.477 nm (*arrows*), and the first intensity maximum of the broad, small angle reflection (obscured somewhat by central scatter) was at 5.9 nm spacing (*arrowheads*).

FTIR Spectra of PrP-(82–146)$_{wt}$ Assemblies Suggest Parallel β-Sheet Organization of Fibrils—FTIR analysis was carried out on PrP-(82–146)$_{wt}$ and PrP-(82–146)$_{106-126scr}$ aggregates because only these peptides formed significant amounts of sedimentable precipitate enabling the preparation of discrete quantities of samples. Fig. 8*A* shows two diagnostic regions of the FTIR spectrum recorded for PrP-(82–146)$_{wt}$ fibrils. The narrow peak 1 that falls at 1630 cm^{-1} (amide I region) indicates the presence of an extended β−sheet structure that arises from symmetric carbonyl stretch (34). The absence of the diagnostic

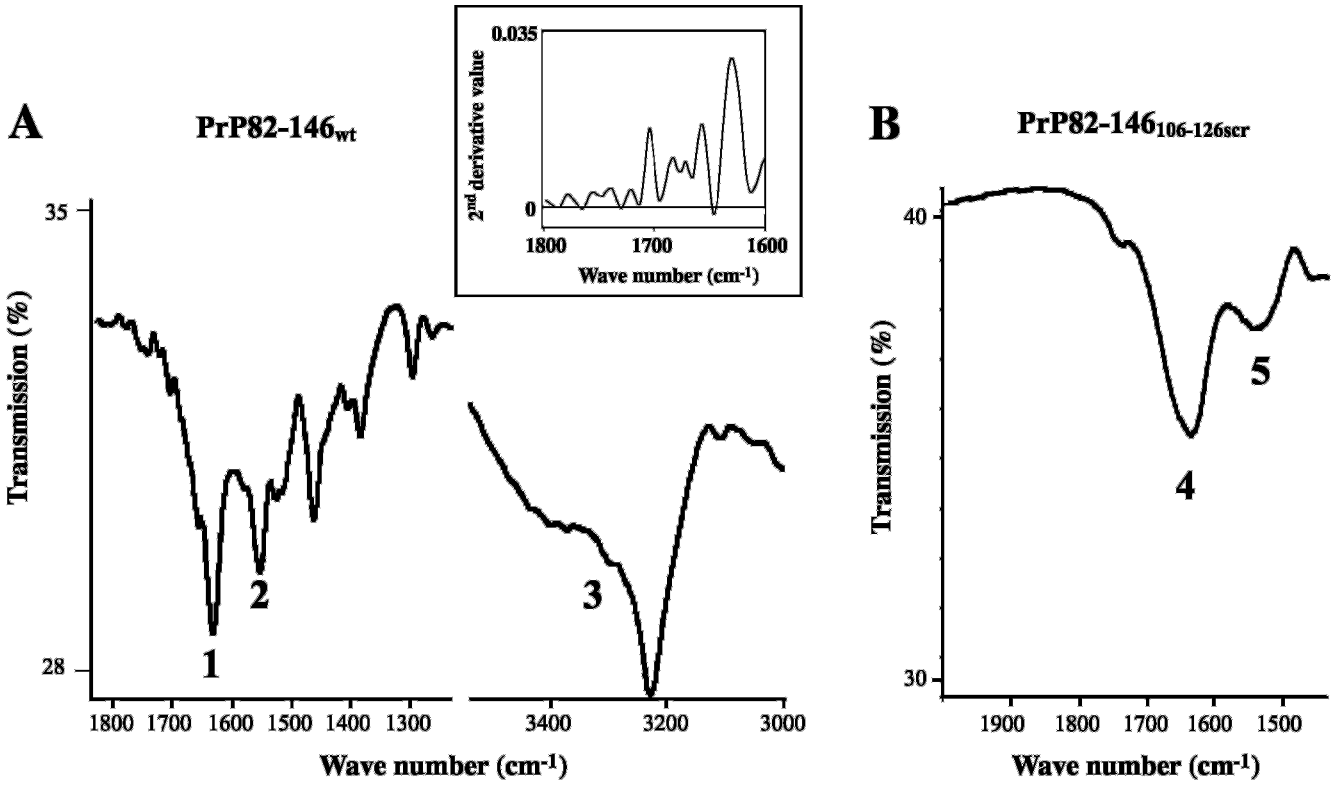

FIG. 8. **FTIR spectra of fibrils formed by PrP-(82–146)$_{wt}$ (*A*) and PrP-(82–146)$_{106–126scr}$ (*B*).** *A*, symmetric carbonyl stretch (*1*), N-H bond deformation (*2*), and N-H symmetric stretch (*3*) bands of PrP-(82–146)$_{wt}$. *Inset*, second derivative of spectrum in range 1600–1800 cm^{-1}. *B*, symmetric carbonyl stretch (*4*), N-H bond deformation (*5*) bands of PrP-(82–146)$_{106–126scr}$.

peak for an anti-parallel β-sheet (1675–1695 cm^{-1}) suggests a parallel β-sheet organization of fibrils (34). Bands 2 and 3 are also indicative of the presence of β-sheet structures; band 2 (ν = 1535 cm^{-1}) arises from the N-H bond deformation (amide II region), and band 3 (ν = 3400 cm^{-1}), which is partially hidden by residual H_2O stretching vibration band, is generated by N-H symmetric stretch. Fig. 8*B* shows the spectrum of PrP-(82–146)$_{106–126scr}$. Peaks 4 (ν = 1634 cm^{-1}) and 5 (ν = 1532 cm^{-1}) indicate the presence of β-sheet structure, but their broadness is suggestive of the presence of multiple conformations. The peak homologous to band 3 in the spectrum of PrP-(82–146)$_{106–126scr}$ is absent, probably covered by stronger absorption of H_2O. The amide I infrared bands were quantitatively resolved to identify the bands corresponding to the different secondary structures present in PrP-(82–146) aggregates. The analysis indicated that PrP-(82–146)$_{wt}$ is primarily composed of β-sheet (54%), with significant amounts of α-helix (22%) and turn (31%). PrP-(82–146)$_{106–126scr}$ showed a content of β-sheet (52%) and α-helix (22%) similar to the wild type sequence; conversely, this peptide had a lower content of turn (17%) and an appreciable amount of random coil (8%) (Table III).

TABLE III
Secondary structures of PrP peptide aggregates as determined by amide I second-derivative analysis
Each value is the mean ± S.D. of three different experiments.

Peptide	Secondary structure			
	α-Helix	β-Sheet	Turn	Random coil
	%			
PrP-(82-146)$_{wt}$	22 ± 5	54 ± 7	24 ± 4	<2
PrP-(82-146)$_{106-126scr}$	23 ± 7	52 ± 8	17 ± 4	8 ± 3

PrP-(82–146)$_{wt}$ Increases Membrane Microviscosity; This Effect Is Dependent upon Integrity of C-terminal Region—The ability of PrP-(82–146)$_{wt}$ and its analogues to affect membrane microviscosity was investigated on suspensions of primary rat cortical neurons using 1,6-diphenyl-1,3,5-hexatriene (DPH) fluorescent probe. Measurements were taken after 30 min of incubation with 25 μM of each peptide and the fluorescence polarization (FP) values were compared with the basal values. In our experimental conditions, because the peptides were immediately tested after solubilization, they were not likely to be highly aggregated (31). The membrane microviscosity was remarkably increased by PrP-(82–146)$_{wt}$ and PrP-(82–146)$_{106–126scr}$ (27.0 and 23.2%, respectively), whereas PrP-(82–146)$_{127–146scr}$ caused a less pronounced effect (16.1%). PrP-(82–146)$_{scr}$ did not change significantly the FP value compared with control conditions. The shorter peptides PrP-(106–126) and PrP-(127–146) were also assayed as positive and negative controls, respectively. As expected, PrP-(106–126) caused a remarkable increase in membrane microviscosity of primary rat cortical neurons, which was significantly higher than that caused by PrP-(82–146)$_{wt}$ and congeners, whereas PrP-(127–146) was totally inactive (Table IV).

DISCUSSION

This work stems from previous findings that the major component of amyloid fibrils of GSS disease is a 7-kDa peptide spanning residues 81–82 and 144–153 of PrP (13, 14). On this basis we generated a synthetic peptide homologous to PrP residues 82–146 to be used for *in vitro* studies, because evidence suggests that the characterization of the physicochemical properties and biological activity of this fragment may help with understanding the pathobiology of GSS as well as of Creutzfeldt-Jakob disease and other transmissible spongiform encephalopathies. According to NMR data on recombinant PrP, the N-terminal two-thirds of this sequence are flexible and

largely unordered, and the C-terminal part contains a short β-strand (35, 36). In GSS disease, this peptide forms insoluble quaternary structures with extensive β-sheet conformation. Furthermore, in Creutzfeldt-Jakob disease and related disorders, residues 82–97 constitute the N terminus of the protease-resistant core of PrP^{Sc} (1, 37), suggesting that also in these conditions the 82–146 sequence undergoes, entirely or in part, a profound physicochemical change. It is noteworthy that most of this region is required for prion propagation, because PrP^{Sc} formation is inhibited by deletion of residues 95–108, 108–122, and 122–141 (18).

The synthetic peptide PrP-$(82–146)_{wt}$ readily formed fibrillar structures whose staining properties and ultrastructure were similar to those of *in situ* amyloid (Table V). EM analysis showed that in the first 24 h the peptide assemblies comprised two populations of fibrils having a diameter of 5.5 and 9.5 nm, respectively. The former prevailed after 1 h of incubation, whereas the latter became the predominant structure after 1 day and was the only form at later stages. This suggests that PrP-(82–146) aggregation is a stepwise process starting with formation of protofilaments which combine to produce the amyloid fibril.

X-ray diffraction measurements of PrP-$(82–146)_{wt}$ showed a low angle reflection at 5.9 nm which we interpreted as arising from the Fourier transform of an ~7–10-nm diameter solid cylinder or tubular structure. This estimate is in good agreement with the electron microscopic measurements of the mature fibrils, as shown in the current study. However, previous studies on better oriented, similar peptides, *i.e.* SHa-(90–145) (33) and Mo-(89–143) carrying the GSS mutation P101L, and a shorter peptide SHa-(104–122) (A113V, A115V, and A118V) (38), reported x-ray evidence for close contact between 4-nm-wide cross-β-fibrils. This suggests that in the less-ordered sample of the current study, a few 4-nm-wide protofilaments are laterally aggregated to constitute a single 7–10-nm-wide fibril. Our current EM study for assemblies of PrP-$(82–146)_{wt}$ showed protofilaments with a similar size (5.5 nm). This dimension indicates that in the assembly, the peptide must be folded, because an extended β-strand at ~0.33 nm per residue would be >20 nm, which is much larger than the protofilament width. X-ray fiber diffraction from related PrP peptides shows intramolecular turns and interactions between domains (39, 40). FTIR analysis showed that PrP-$(82–146)_{wt}$ had a parallel β-structure, and a second derivative of infrared spectra indicated that peptide aggregates are primarily composed of β-sheet (54%) and -turn (24%) which is consistent with their amyloid-like properties. Moreover, the absence of loosely wound random coil structures accounts for the resistance of PrP-$(82–146)_{wt}$ to protease digestion.

PrP-$(82–146)_{wt}$ showed the ability to interact with plasma membranes of neuronal cells, resulting in remarkable increase in membrane microviscosity. A similar effect was previously observed with peptide fragments of this sequence (*i.e.* PrP-(106–126) and PrP-(118–135)) (31, 41) and might be relevant to disease pathogenesis, because cultured neurons exposed to PrP^{Sc} exhibit increased membrane microviscosity (42). It is conceivable that this interaction affects membrane homeostasis and plays a significant role in nerve cell dysfunction and death that occurs in prion disease (43). This view is supported by the observation that the exposure of primary neuronal cultures to micromolar concentration of PrP-(82–146) results in apoptotic cell death which is largely independent from the expression of endogenous PrP.

Previous studies (20–22) with short synthetic peptides homologous to consecutive segments of PrP-(82–146) showed that the sequence spanning residues 106–126 has the highest propensity to adopt stable β-sheet structure and assemble into amyloid fibrils that are ultrastructurally similar to those observed in GSS patients. Also the peptide PrP-(127–147) was able to generate filamentous structures resembling the scrapie-associated fibrils isolated from humans and animals with transmissible spongiform encephalopathy. However, this peptide had a lower amyloidogenic potential than PrP-(106–126) and was required to be intact, as shorter peptides spanning residues 127–135 or 135–147 were non-fibrillogenic (20). A further difference between these peptides was that PrP-(106–126) was highly toxic to primary neuronal cultures, whereas PrP-(127–147) had minor effects on cell survival (44). To verify the relative contribution of these sequences to the physicochemical properties of the GSS amyloid protein, we synthesized PrP-(82–146) analogues with a selective alteration of the 106–126 or the 127–146 region. Either change remarkably affected the characteristics of PrP-(82–146), although with divergent effects. PrP-$(82–146)_{106–126scr}$ showed an increased aggregation rate in the first 24 h. However, the peptide assemblies mainly consisted of granular and amorphous material and were largely resistant to protease digestion. Noteworthy, the fraction of peptide that was not recruited into this fast process still had the ability to generate fibrillar structures with the tinctorial properties of amyloid. Conversely, PrP-$(82–146)_{127–146scr}$ showed a remarkable decrease in aggregation ability and protease

TABLE IV
Effects of PrP peptides on plasma membrane microviscosity of cortical neuronal cells as deduced from FP values

Each value is the mean ± S.D. of three different experiments.

Peptide	FP value	Increase
	arbitrary units	%
None	0.267 ± 0.002	
PrP-$(82-146)_{wt}$	0.339 ± 0.001[a]	27.0
PrP-$(82-146)_{106-126scr}$	0.329 ± 0.001[a]	23.2
PrP-$(82-146)_{127-146scr}$	0.310 ± 0.002[a]	16.1
PrP-$(82-146)_{scr}$	0.289 ± 0.001	8.2
PrP-(106-126)	0.398 ± 0.002[a]	49.1
PrP-(127-146)	0.269 ± 0.001	<1

[a] $p < 0.01$, Duncan's test *versus* basal value, $n = 5$.

TABLE V
Features of PrP-(82-146) analogues

PrP peptide	PrP-$(82-146)_{wt}$	PrP-$(82-146)_{106-126scr}$	PrP-$(82-146)_{127-146scr}$	PrP-$(82-146)_{scr}$
β-Sheet content (%)[a]	54	52	ND[b]	ND
Aggregation after 96 h (%)	90	85	12	0
PK-resistant fraction (%)	47	78	15	4
X-ray diffraction patterns[c]	β	β	−	−
Assemblies after 168 h				
Amyloid fibrils	+++	+	±	−
Amorphous aggregates	−	+++	++	−
Increase in membrane micoviscosity (%)	27	23	16	8

[a] Determined in peptide aggregates by FTIR.
[b] ND, not determined.
[c] β, presence of the ~0.47-nm Bragg spacing typical of β-sheet conformation in amyloids; −, no scatter detected, suggesting lack of sufficient amounts of organized macromolecular assemblies for detection by x-ray diffraction.

resistance and was essentially incapable of forming amyloid fibrils. Despite these differences, both peptides increased the plasma membrane microviscosity, although this effect was more pronounced for PrP-(82–146)$_{106–126scr}$. Overall, these data indicate that both sequences are important determinants of the physicochemical properties of PrP-(82–146), although in the intact amyloid peptide the contribution of the C-terminal segment seems to be essential, because the modification of the 127–146 region had the most profound effect on secondary structure and aggregation. This is likely due to the difference in charge distribution between PrP-(82–146)$_{127–146scr}$ and PrP-(82–146)$_{wt}$, suggesting that assembly of the wild type peptide into fibrillar β-sheet structures is driven by electrostatic interactions between Asp/Glu residues at the C-terminal end and Lys residues in the N-terminal half of polypeptide chains.

The intrinsic physicochemical properties of PrP-(82–146)$_{wt}$ account for the massive deposition of PrP amyloid in GSS (7). This peptide corresponds to a PrP region that undergoes a major conformational change in $PrP^{C} \rightarrow PrP^{Sc}$ transition and is required for infectivity (1, 18). Accordingly, it should be regarded as a prime tool for investigating the molecular basis of protein misfolding and aggregation and disease pathogenesis. Availability of wild type and modified sequences could be conveniently used for large scale screening of compounds capable of binding selectively to this critical domain and destabilizing the β-sheet structure.

REFERENCES

1. Prusiner, S. B. (1991) *Science* **252,** 1515–1522
2. Prusiner, S. B., Scott, M. R., DeArmond, S. J., and Cohen, F. E. (1998) *Cell* **93,** 337–348
3. Caughey, B. W., Dong, A., Bhat, K. S., Ernst, D., Hayes, S. F., and Caughey, W. S. (1991) *Biochemistry* **30,** 7672–7680
4. Pan, K. M., Baldwin, M., Nguyen, J., Gasset, M., Serban, A., Groth, D., Mehlhorn, I., Huang, Z., Fletterick, R. J., Cohen, F. E., and Prusiner, S. B. (1993) *Proc. Natl. Acad. Sci. U. S. A.* **90,** 10962–10966
5. Safar, J., Roller, P. P., Gajdusek, D. C., and Gibbs, C. J., Jr. (1993) *J. Biol. Chem.* **268,** 20276–20284
6. Prusiner, S. B., McKinley, M. P., Bowman, K. A., Bolton, D. C., Bendheim, P. E., Groth, D. F., and Glenner, G. G. (1983) *Cell* **35,** 349–358
7. Ghetti, B., Piccardo, P., Frangione, B., Bugiani, O., Giaccone, G., Young, K., Prelli, F., Farlow, M. R., Dlouhy, S. R., and Tagliavini, F. (1996) *Brain Pathol.* **6,** 127–145
8. Ghetti, B., Piccardo, P., Spillantini, M. G., Ichimiya, Y., Porro, M., Perini, F., Kitamoto, T., Tateishi, J., Seiler, C., Frangione, B., Bugiani, O., Giaccone, G., Prelli, F., Goedert, M., Dlouhy, S. R., and Tagliavini, F. (1996) *Proc. Natl. Acad. Sci. U. S. A.* **93,** 744–748
9. Will, R. G., Ironside, J. W., Zeidler, M., Cousens, S. N., Estibeiro, K., Alperovitch, A., Poser, S., Pocchiari, M., Hofman, A., and Smith, P. G. (1996) *Lancet* **347,** 921–925
10. Bruce, M. E., Will, R. G., Ironside, J. W., McConnell, I., Drummond, D., Suttie, A., McCardle, L., Chree, A., Hope, J., Birkett, C., Cousens, S., Fraser, H., and Bostock, C. J. (1997) *Nature* **389,** 498–501
11. Giaccone, G., Verga, L., Bugiani, O., Frangione, B., Serban, D., Prusiner, S. B., Farlow, M. R., Ghetti, B., and Tagliavini, F. (1992) *Proc. Natl. Acad. Sci. U. S. A.* **89,** 9349–9353
12. Tagliavini, F., Prelli, F., Ghiso, J., Bugiani, O., Serban, D., Prusiner, S. B., Farlow, M. R., Ghetti, B., and Frangione, B. (1991) *EMBO J.* **10,** 513–519
13. Tagliavini, F., Prelli, F., Porro, M., Rossi, G., Giaccone, G., Farow, M. R., Dlouhy, S. R., Ghetti, B., Bugiani, O., and Frangione, B. (1994) *Cell* **79,** 695–703
14. Tagliavini, F., Lievens, P. M., Tranchant, C., Warter, J. M., Mohr, M., Giaccone, G., Perini, F., Rossi, G., Salmona, M., Piccardo, P., Ghetti, B., Beavis, R. C., Bugiani, O., Frangione, B., and Prelli, F. (2001) *J. Biol. Chem.* **276,** 6009–6015
15. Piccardo, P., Seiler, C., Dlouhy, S. R., Young, K., Farlow, M. R., Prelli, F., Frangione, B., Bugiani, O., Tagliavini, F., and Ghetti, B. (1996) *J. Neuropathol. Exp. Neurol.* **55,** 1157–1163
16. Piccardo, P., Dlouhy, S. R., Lievens, P. M., Young, K., Bird, T. D., Nochlin, D., Dickson, D. W., Vinters, H. V., Zimmerman, T. R., Mackenzie, I. R., Kish, S. J., Ang, L. C., De Carli, C., Pocchiari, M., Brown, P., Gibbs, C. J., Jr., Gajdusek, D. C., Bugiani, O., Ironside, J., Tagliavini, F., and Ghetti, B. (1998) *J. Neuropathol. Exp. Neurol.* **57,** 979–988
17. Parchi, P., Chen, S. G., Brown, P., Zou, W., Capellari, S., Budka, H., Hainfellner, J., Reyes, P. F., Golden, G. T., Hauw, J. J., Gajdusek, D. C., and Gambetti, P. (1998) *Proc. Natl. Acad. Sci. U. S. A.* **95,** 8322–8327
18. Muramoto, T., Scott, M., Cohen, F. E., and Prusiner, S. B. (1996) *Proc. Natl. Acad. Sci. U. S. A.* **93,** 15457–15462
19. Supattapone, S., Bosque, P., Muramoto, T., Wille, H., Aagaard, C., Peretz, D., Nguyen, H. O., Heinrich, C., Torchia, M., Safar, J., Cohen, F. E., DeArmond, S. J., Prusiner, S. B., and Scott, M. (1999) *Cell* **96,** 869–878
20. Tagliavini, F., Prelli, F., Verga, L., Giaccone, G., Sarma, R., Gorevic, P., Ghetti, B., Passerini, F., Ghibaudi, E., Forloni, G., Salmona, M., Bugiani, O., and Frangione, B. (1993) *Proc. Natl. Acad. Sci. U. S. A.* **90,** 9678–9682
21. Selvaggini, C., De Gioia, L., Cantù, L., Ghibaudi, E., Diomede, L., Passerini, F., Forloni, G., Bugiani, O., Tagliavini, F., and Salmona, M. (1993) *Biochem. Biophys. Res. Commun.* **194,** 1380–1386
22. De Gioia, L., Selvaggini, C., Ghibaudi, E., Diomede, L., Bugiani, O., Forloni, G., Tagliavini, F., and Salmona, M. (1994) *J. Biol. Chem.* **269,** 7859–7862
23. Tagliavini, F., Forloni, G., Colombo, L., Rossi, G., Girola, L., Canciani, B., Angeretti, N., Giampaolo, L., Peressini, E., Awan, T., De Gioia, L., Ragg, E., Bugiani, O., and Salmona, M. (2000) *J. Mol. Biol.* **300,** 1309–1322
24. Kyte, J., and Doolittle, R. F. (1982) *J. Mol. Biol.* **157,** 105–132
25. Krogh, A., Larsson, B., von Heijne, G., and Sonnhammer, E. L. (2001) *J. Mol. Biol.* **305,** 567–580
26. Salmona, M., Malesani, P., De Gioia, L., Gorla, S., Bruschi, M., Molinari, A., Della Vedova, F., Pedrotti, B., Marrari, M. A., Awan, T., Bugiani, O., Forloni, G., and Tagliavini, F. (1999) *Biochem. J.* **342,** 207–214
27. Oldenbourgh, R., and Phillips, W. C. (1986) *Rev. Sci. Instrum.* **57,** 2362–2365
28. Makowski, L. (1989) in *Brookhaven Symposium, Synchrotron Radiation in Biology* (Sweet, R. M., and Woodhead, A. D., eds) pp. 341–347, Plenum Publishing Corp., New York
29. Cantor, C. R., and Schimmel, P. R. (1980) *Biophysical Chemistry,* Part II, pp. 468–477, W. H. Freeman & Co., New York
30. Nillson, M. R., and Dobson, C. M. (2003) *Biochemistry* **42,** 375–382
31. Salmona, M., Forloni, G., Diomede, L., Algeri, M., De Gioia, L., Angeretti, N., Giaccone, G., Tagliavini, F., and Bugiani, O. (1997) *Neurobiol. Dis.* **4,** 47–57
32. Inouye, H., Fraser, P. E., and Kirschner, D. A. (1993) *Biophys. J.* **64,** 502–519
33. Inouye, H., and Kirschner, D. A. (1997) *J. Mol. Biol.* **268,** 375–389
34. Balbimie, M., Grothe, R., and Eisenberg, D. S. (2001) *Proc. Natl. Acad. Sci. U. S. A.* **98,** 2375–2380
35. Riek, R., Hornemann, S., Wider, G., Glockshuber, R., and Wuthrich, K. (1997) *FEBS Lett.* **413,** 282–288
36. Zahn, R., Liu, A., Luhrs, T., Riek, R., von Schroetter, C., Lopez Garcia, F., Billeter, M., Calzolai, L., Wider, G., and Wuthrich, K. (2000) *Proc. Natl. Acad. Sci. U. S. A.* **97,** 145–150
37. Parchi, P., Zou, W., Wang, W., Brown, P., Capellari, S., Ghetti, B., Kopp, N., Schulz-Schaeffer, W. J., Kretzschmar, H. A., Head, M. W., Ironside, J. W., Gambetti, P., and Chen, S. G. (2000) *Proc. Natl. Acad. Sci. U. S. A.* **97,** 10168–10172
38. Inouye, H., Bond, J., Baldwin, M. A., Ball, H. L., Prusiner, S. B., and Kirschner, D. A. (2000) *J. Mol. Biol.* **300,** 1283–1296
39. Inouye, H., and Kirschner, D. A. (1998) *J. Struct. Biol.* **122,** 247–255
40. Inouye, H., and Kirschner, D. A. (2003) *Fibre Diffract. Rev.* **11,** 102–112
41. Pillot, T., Lins, L., Goethals, M., Vanloo, B., Baert, J., Vandekerckhove, J., Rosseneu, M., and Brasseur, R. (1997) *J. Mol. Biol.* **274,** 381–393
42. Kristensson, K., Feuerstein, B., Taraboulos, S., Hyun, W. C., Prusiner, S. B., and De Armond, S. J. (1993) *Neurology* **43,** 2335–2341
43. Tagliavini, F., Forloni, G., D'Ursi, P., Bugiani, O., and Salmona, M. (2001) *Adv. Protein Chem.* **57,** 171–201
44. Forloni, G., Angeretti, N., Chiesa, R., Monzani, E., Salmona, M., Bugiani, O., and Tagliavini, F. (1993) *Nature* **362,** 543–546